

Supramolecular Chirality in Organo-, Hydro-, and Metallogels Derived from Bis-amides of L-(+)-Tartaric Acid: Formation of Highly Aligned 1D Silica Fibers and Evidence of 5-c Net SnS Topology in a Metallogel Network

Uttam Kumar Das and Parthasarathi Dastidar*^[a]

Abstract: A series of bis-amides derived from L-(+)-tartaric acid was synthesized as potential low-molecular-weight gelators. Out of 14 bis-amides synthesized, 13 displayed organo-, hydro-, and ambidextrous gelation behavior. The gels were characterized by methods including circular dichroism, differential scanning calorimetry, optical and electron microscopy, and rheology. One of the gels derived from di-3-pyridyltartaramide (**D-3-PyTA**) dis-

played intriguing nanotubular morphology of the gel network, which was exploited as a template to generate highly aligned 1D silica fibers. The gelator **D-3-PyTA** was also exploited to generate metallogels by treatment with various Cu^{II}/Zn^{II} salts under suitable

Keywords: amides • gels • supramolecular chemistry • tartaric acid • X-ray diffraction

conditions. A structure–property correlation on the basis of single-crystal and powder X-ray diffraction data was attempted to gain insight into the structures of the gel networks in both organo- and metallogels. Such study led to the determination of the gel-network structure of the Cu^{II} coordination-polymer-based metallogel, which displayed a 2D sheet architecture made of a chloride-bridged double helix that resembled a 5-c net SnS topology.

Introduction

Low-molecular-mass organic gelators (LMOG) are small organic molecules that can entrap a large volume of solvent, thus resulting in solidlike viscoelastic materials.^[1] The anisotropic supramolecular (noncovalent) interactions (such as hydrogen bonding, van der Waals forces, π – π interactions, and so on) among the gelator molecules lead to the highly directional metastable self-assembled fibrillar networks (SAFINs).^[2] The SAFINs are further entangled to form a 3D network within which the solvent molecules are immobilized by means of surface tension. For the last two decades, research activities on supramolecular gels have increased because of their potential applications in, for example, conservation of art,^[3] electro-optics/photronics,^[4] structure-directing agents,^[5] cosmetics,^[6] drug delivery,^[7] biomedical applications,^[8] sensors,^[9] oil recovery,^[10] catalysis,^[11] and so on. For various reasons, such as wide structural diversities in known gelator molecules (cholesterol and anthracene derivatives,^[9a,12] surfactants,^[13,27] porphyrins and phthalocyanines,^[14,42a] carbohydrates^[15] and peptide derivatives,^[16] bis-urea derivatives,^[17] and so on) or a lack of molecular-level understanding of the gelation mechanism, it is difficult to design a

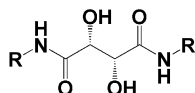
priori a gelator molecule. Nevertheless, there have been efforts by various groups to design gelator molecules. Weiss et al. have designed a series of aromatic linker steroid (ALS)-based gelators by rationalizing the observations of existing literature.^[2] van Esch et al. reported C₃-symmetric hydrogelator derivatives wherein the critical balance of hydrophobicity and hydrophilicity were rationally introduced to effect hydrogelation.^[18] Our group has shown that the supramolecular synthon approach is quite successful in designing organic-salt-based gelators.^[19]

Chiral gels that represent supramolecular chirality are important in chiro-optical switches,^[20] chiral catalysis,^[21] helical crystallization of proteins^[22] and inorganic replicas,^[5] chiral resolution,^[23] and so on. We have been engaged in developing easily accessible chiral gels.^[24] Amide functionality is known to impart gelation in many gelators reported.^[25] It is believed that the self-complementary 1D hydrogen-bonding interactions of secondary amide^[26] lead to gel formation. L-(+)-Tartaric acid (TA) is a commercially available and inexpensive chiral source. We have therefore decided to exploit TA by installing amide functionality. Surprisingly, there is no amide-based gelator that has been derived from TA reported in the literature. Oda et al., however, reported gels derived from gemini surfactants derived from TA-based salts.^[27]

In this paper we report a series of TA-based bis-amide gelators (Scheme 1). The amides were characterized by FTIR, ¹H and ¹³C NMR spectroscopy, and HRMS. Most of the amides showed gelation properties. Compound **D-3-PyTA** showed interesting metallogelation behavior. Single-crystal structures of three gelator and one nongelator molecules have also been reported. The gels were characterized by dif-

[a] U. K. Das, Dr. P. Dastidar
Department of Organic Chemistry
Indian Association for the Cultivation of Science (IACS)
2A and 2B, Raja S. C. Mullick Road
Jadavpur, Kolkata, 700032, West Bengal (India)
Fax: (+91) 33-2473-2805
E-mail: ocpd@iacs.res.in

Supporting information for this article is available on the WWW under <http://dx.doi.org/10.1002/chem.201200871>.



R = -(CH ₂) ₃ -CH ₃ ,	DBuTA ;	-(CH ₂) ₄ -CH ₃ ,	DPenTA
-(CH ₂) ₅ -CH ₃ ,	DHexTA ;	-(CH ₂) ₆ -CH ₃ ,	DHepTA
-(CH ₂) ₇ -CH ₃ ,	DOctTA ;	-(CH ₂) ₈ -CH ₃ ,	DNonTA
-(CH ₂) ₉ -CH ₃ ,	DDTA ;	-(CH ₂) ₁₀ -CH ₃ ,	DUnDTA
-(CH ₂) ₁₁ -CH ₃ ,	DDDTA ;	-(CH ₂) ₁₃ -CH ₃ ,	DTDTA
-3-pyridyl,	D-3-PyTA ;	-phenyl,	DPhTA
-4-methoxyphenyl,	B-4-MPhTA ;	-4-nitrophenyl,	B-4-NPhTA

Scheme 1. Bis-amides of L-(+)-tartaric acid.

ferential scanning calorimetry (DSC), rheology, scanning and transmission electron microscopy (SEM, TEM). Structure–property correlation has been attempted in some selected cases by using powder and single-crystal X-ray diffraction (PXRD, SXRD).

Results and Discussion

Gelation studies: All the compounds were prepared following a modified literature procedure^[28] (see the Experimental Section). The compounds were scanned for gelation properties with 18 prototype solvents, both polar and nonpolar (Table S15 in the Supporting Information).

All the gels (confirmed by the test-tube inversion method^[29]) were thermoreversible and stable for months under ambient conditions. Many of the gelators showed ambidextrous (i.e., capable of gelling both organic and aqueous solvents) gelling behavior. When the terminal substituents were *n*-alkyl chains, the gelation abilities of the corresponding bis-amide derivatives were quite versatile and displayed the ability to gel most of the solvents studied herein. Interestingly, when the terminal substituents were replaced with aromatic moieties, the gelation behavior of the corresponding compounds changed drastically. Whereas 3-pyridyl (**D-3-pyTA**) and 4-nitro (**B-4-NPhTA**) derivatives displayed only hydrogelation, the corresponding phenyl derivative (**DPhTA**) was found to be a nongelator, and the 4-methoxy derivative (**B-4-MPhTA**) displayed ambidextrous behavior. The role of the pyridyl N in gelation was probed by carrying out gelation of **D-3-pyTA** in a solution of DMF/water with pH of varying acidity. It was observed that **D-3-pyTA** failed to produce gel below pH 7.0 (Figure S1 in the Supporting information), thus indicating possible protonation of the pyridyl N atom and thereby disruption of the hydrogen bonding, which is presumably responsible for the formation of the desired SAFIN required for gelation. The minimum gelator concentration (MGC) and the gel dissociation temperature T_{gel} were within the range of 0.35–4 wt % and 56–120 °C, respectively, thus indicating significant efficiency and

thermal stability of the gels. Figure 1 depicts the plot of T_{gel} versus [Gelator] wherein the gels were prepared in a binary mixture of DMF and water with varying concentrations of

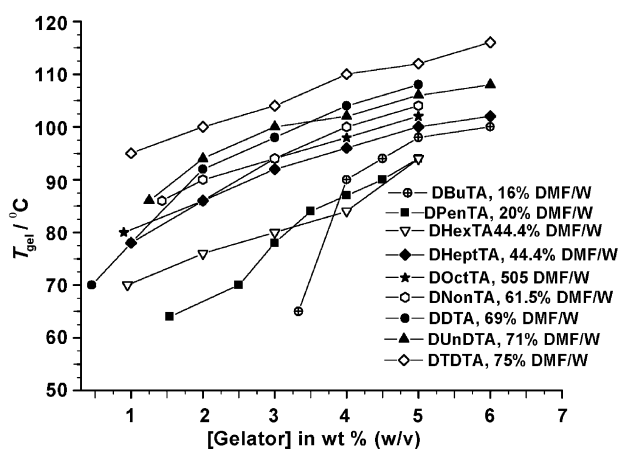


Figure 1. T_{gel} versus [Gelator] plots for some selected gels.

DMF (total volume = 0.5 mL). The T_{gel} gradually increased with [Gelator], which means that the gel-forming networks were governed by supramolecular interactions (presumably hydrogen-bonding, alkyl–alkyl hydrophobic interactions). The fact that the hydrophobic interactions that involve the alkyl chains indeed played a crucial role in gelation was clear from the highest T_{gel} of the gel derived from the gelator with the longest alkyl chain (**DTDTA**).

Calorimetric characterization of two selected gels derived from the gelators with the longest and shortest alkyl chains (**DTDTA** and **DBuTA**, respectively) in the series showed intriguing results (Figure 2).

In both the cases, there were two peaks in each endothermic and exothermic run. The peaks in **DTDTA** gel were much sharper than those in **DBuTA** gel, which could be due to the stronger gel strength of the DMSO gel of **DTDTA**. Since the existence of two peaks in each run might indicate solvotropic liquid-crystalline (LC) behavior,^[30] we examined these gels under hot-stage optical microscopy. However, the microscopic observations did not support the formation of LC phases (Figure S2 in the Supporting Information). Thus, the peaks at 91 and 103 °C for DMSO and toluene gel of **DTDTA** and **DBuTA**, respectively, could be due to the crystalline phase change of the SAFINs during gel–sol transition; the other two peaks at 106 and 86 °C in respective cases represented the gel–sol transition (Figure 1).

Since it is difficult to assess the enthalpy change (ΔH) associated with the process of the gel–sol transition because of the generally observed broad peaks in the endotherm of the DSC traces, we made an attempt to extract the ΔH values associated with a gel–sol transition from the T_{gel} versus [Gelator] plot (Figure 1).^[31] Interestingly, when the semilog of the mole fraction of each gelator at each concentration extracted from Figure 1 was plotted against $1/T_{\text{gel}}\text{K}^{-1}$, nice

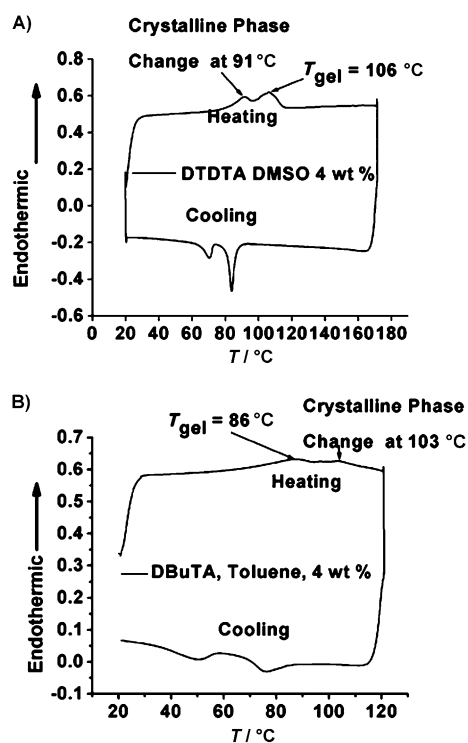


Figure 2. DSC traces of A) approximately 4.0 wt% DMSO gel of **DTDTA**; B) approximately 4.0 wt% toluene gel of **DBuTA**.

linear plots were obtained that represented the Schroeder-van Laar equation [Eq. (1), Figure 3].^[32]

$$\ln[\text{gelator}] = -(\Delta H_m / RT_{\text{gel}}) + \text{constant} \quad (1)$$

in which ΔH_m is the enthalpy of melting and T_{gel} is the transition temperature of the gel-sol transition, which means that the gel-sol transition can be considered a first-order transition if we consider that the gel melts into an ideal solu-

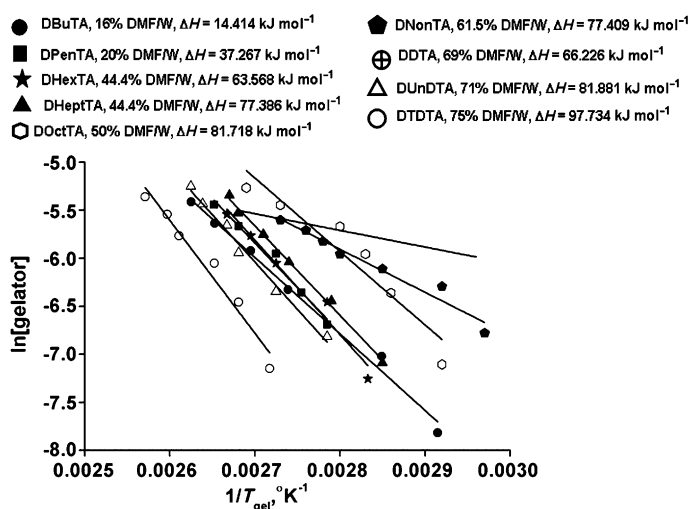


Figure 3. Semilog plot of the mole fraction of the gelators against $1/T$.

tion and a definite amount of gelator is involved in the phase transition. From the plots, the enthalpy ΔH_m was calculated to be within the range of $14.4\text{--}97.7 \text{ kJ mol}^{-1}$.

Microscopy: SEM micrographs of the DMF/water xerogels of some selected gelators revealed interesting results. In the cases of alkyl-substituted gelators, the corresponding xerogels displayed discrete plate (**DBuTA**, **DPenTA**, **DNonTA**, **DUnDTA**, **DTDTA**), discrete tape (**B-4-MPhTA**), and highly entangled tape (**DHexTA**, **DDTA**) morphologies. The most intriguing morphology was observed in the case of **D-3-PyTA**, wherein highly aligned nanotubes could be seen. The presence of nanotubular morphology also was confirmed in highly reproducible TEM images (Figure 4). This

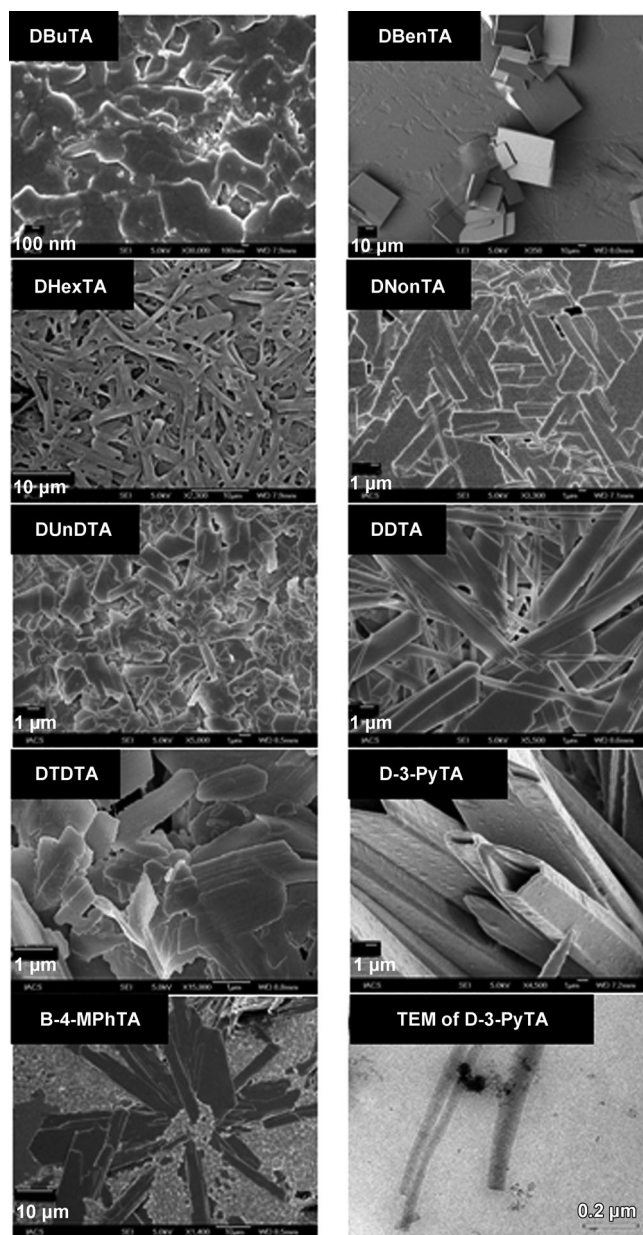


Figure 4. SEM of selected xerogels and TEM of the xerogel of **D-3-PyTA**; all the gels were prepared in DMF/water.

observation prompted us to exploit the nanotubular morphology of the gel network as template^[5] to generate highly aligned 1D fibrous silica from Si(OC₂H₅)₄ (TEOS; Figure S6 in the Supporting Information).

Rheology: Dynamic rheology was carried out on some selected gels to evaluate their gel-like response.^[33] In typical frequency sweep experiments, the elasticity modulus G' and the viscosity modulus G'' were plotted as a function of the angular frequency ' ω ' at a constant strain of 0.01%. In these experiments, 4 wt% DMF/water gels of the gelators with the shortest and longest alkyl chains (DBuTA and DTDTA, respectively) were selected to see the effect of the length of the alkyl chain on the viscoelastic behavior of the corresponding gels. Figure 5 shows that in both the cases the G'

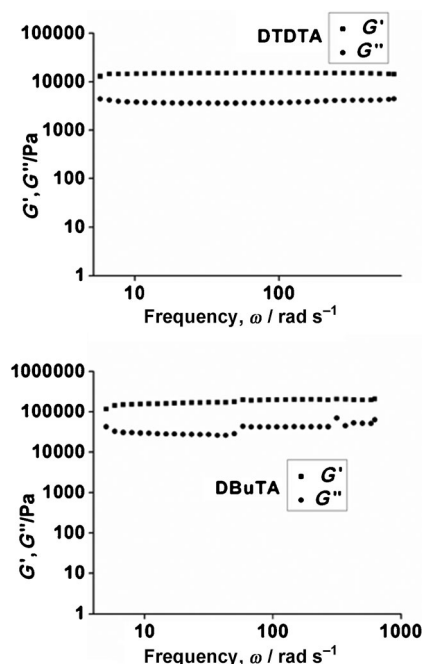


Figure 5. Dynamic rheology of (DMF/water) gels of **DTDTA** and **DBuTA** at 25 °C; the elasticity modulus G' and viscosity modulus G'' are shown as a function of the angular frequency ω . The strain used was 0.01%.

values (191.9 and 15.2 kPa for **DBuTA** and **DTDTA**, respectively) remained frequency-invariant over a considerable period on the timescale and were significantly larger in magnitude than the corresponding G'' values, which supports their gel-like response. It is, however, intriguing to note that the gelator with the shortest alkyl chain in the series displayed better viscoelastic properties than the gelator with the longest alkyl chain. Yield stress experiments with 10 gels (all 4 wt% DMF/water gels) derived from the *n*-alkyl-substituted bis-amide gelators also indicated a similar trend. In this cases, too, **DBuTA** displayed highest yield stress (586 Pa), which gradually decreased as the chain length increased (Figure 6).

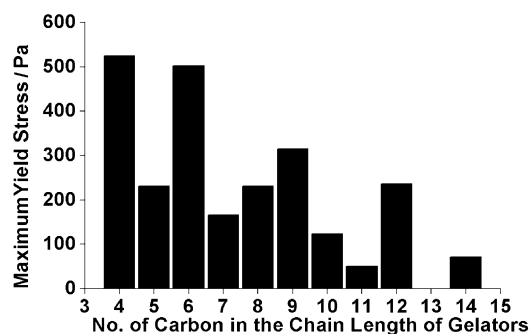


Figure 6. Yield stress versus the number of carbon atoms present in the aliphatic amine of bis-tartaramide derivatives.

These counterintuitive observations could be because of the more crystalline nature of the gel fibers that are derived from the gelators with the shorter alkyl chains (Figure S3 in the Supporting Information). In rotational flow curve experiments, the viscosity of the 4 wt% DMF/water gels of **DBuTA** and **DTDTA** showed a steady decrease as the shear rate increased, which indicates that they were shear-thinning materials (Figure 7). In the cases of aromatic-substituted ge-

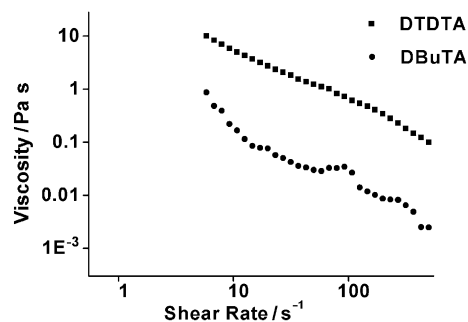


Figure 7. A typical flow curve measurement of gels made in a binary mixture of DMF and water.

lators, namely, **D-3-PyTA**, **B-4-MPhTA**, and **B-4-NPhTA**, the yield stress of the pyridyl-substituted gelator **D-3-PyTA** (4 wt% DMF/water gel) showed maximum yield stress, presumably due to the participation of pyridyl N atoms in hydrogen bonding. Rotational flow curve experiments also showed the expected trend (Figure S4 in the Supporting Information).

Circular dichroism: CD spectra were recorded on two selected gels, namely, **DTDTA** (4 wt% in toluene) and **D-3-PyTA** (4 wt% in DMF/water); the spectra of the corresponding solutions were also obtained. Both the gels and the corresponding solutions displayed a positive Cotton effect. The **DTDTA** gel showed a peak at approximately 223 nm and a trough at approximately 200 nm. The corresponding solution also showed a similar peak and trough near 208 and 198 nm, respectively. On the other hand, **D-3-PyTA** gel showed a peak at approximately 251 nm and a

trough at approximately 224 nm; in the corresponding solution, the peak and trough appeared at approximately 252 and 233 nm, respectively. These CD signals are due to the π - π^* transition of the amide carbonyl, and the patterns are similar to that of the β sheet in polypeptides.^[34] The sharp peaks at approximately 272 and 302 nm in **3-D-PyTA** gel were due to π - π^* and n - π^* transitions of the aromatic (pyridyl) moiety and indicated the higher anisotropy in the gel state. This observation is further supported by the absence of such peaks in the corresponding solution. However, a very sharp peak at approximately 245 nm in the solution of **DTDTA** in toluene was due to the π - π^* transition of the solvent (Figure 8).

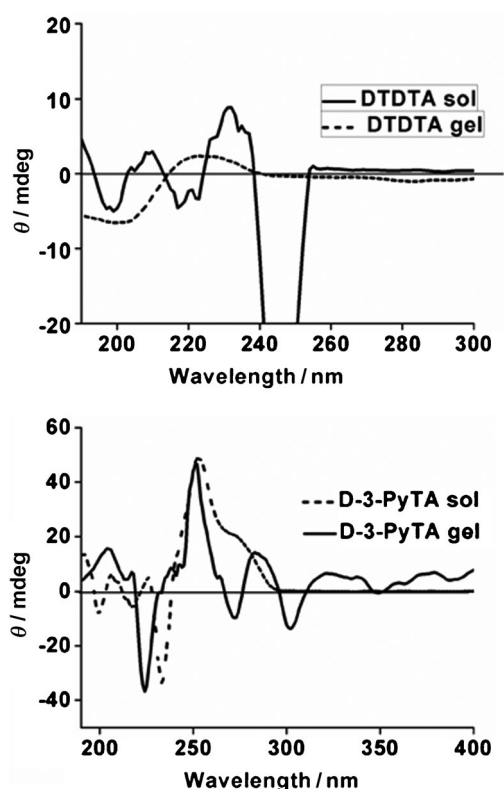


Figure 8. CD spectra of some selected gels and their corresponding sols.

Single-crystal X-ray diffraction: It is believed that the gelation is a frustrated crystallization process wherein the SAFINs are formed from a suitable solution that contains the gelator molecule.^[1] In fact, there are many occasions in which single crystals of the gelator molecules are obtained from aging gel samples.^[35] The implication of the crystal structure of the gelator molecule is enormous in designing gelators.^[19] It was proposed a decade ago that 1D hydrogen-bonded network-promoted gelation and such anisotropic interactions helped the molecules to grow as fibers with a high aspect ratio, which consequently formed SAFINs under suitable conditions to impart gelation. However, 2D or 3D hydrogen-bonded networks either produced weak gel or no gelation at all, and in these cases, the 1D growth of fibers

was somewhat prevented.^[36] This hypothesis was most explicitly demonstrated by our group in various organic-salt-based gelators.^[19,37] Since bis-amide can also participate in the 1D β sheet, we thought it was worthwhile to attempt to determine the crystal structures of the compounds reported herein and correlated their structures with the gelation/nongelation properties. The presence of two hydroxyl groups in the tartaric acid backbone was also expected to participate in hydrogen bonding. With this background, we attempted to crystallize all the compounds reported in this article. Our best efforts resulted in crystallization of four compounds, of which three compounds were gelators (Table S16 in the Supporting Information). The following sections describe the single-crystal structures of the compounds.

Single-crystal structure of DHepTA: This compound was crystallized in the non-centrosymmetric monoclinic space group C_2 , and its asymmetric unit contained one gelator molecule. The chiral backbone of the tartaric acid adopted a conformation wherein the hydroxyl groups were gauche and the amide moieties were staggered with respect to each other. The conformations of the alkyl groups were found to be quite different. Whereas the methylene groups in one of the alkyl chains all showed staggered conformation, the methylene groups in the other alkyl chain displayed gauche conformation. The dihedral angle that involves the two amide moieties was found to be 74.8° , which indicates that they were almost orthogonal to each other. Under such an arrangement, a β sheet that involves the bis-amide moiety could not be formed. Whereas one of the amide N-H groups was involved in complementary hydrogen bonding with the neighboring amide moiety of the adjacent gelator molecule ($N\cdots O = 3.064(4) \text{ \AA}$; $\angle N-H\cdots O = 147.4^\circ$), the N-H of the other amide did not participate in hydrogen-bonding interactions; the $>C=O$ moiety of this amide group was involved in hydrogen bonding with one of the hydroxyl groups of the neighboring molecule ($O\cdots O = 2.617(3) \text{ \AA}$; $\angle O-H\cdots O = 176(11)^\circ$). The other hydroxyl group participated in extended hydrogen-bonding interactions with the crystallographically equivalent hydroxyl groups of the neighboring molecules. The overall hydrogen-bonded network may thus be described as 2D sheet architecture that was further packed in parallel fashion without displaying any alkyl-alkyl interdigitation (Figure 9).

Single-crystal structure of D-3-PyTA: This compound was crystallized in the non-centrosymmetric orthorhombic space group $P2_12_12_1$, and its asymmetric unit contained one molecule. The hydroxyl groups and the terminal amide moieties displayed a gauche and staggered conformation with respect to each other. The relative orientation of the terminal pyridyl N atoms was *anti*, whereas the conformation that involved the pyridyl N and amide O in each terminal was found to be *syn-syn*. The amide pyridyl moiety in each terminal displayed a planar conformation with dihedral angles of 13.3° and 22.0° . The terminal pyridyl rings were found to be coplanar and displayed a dihedral angle of 6.14° . Interestingly,

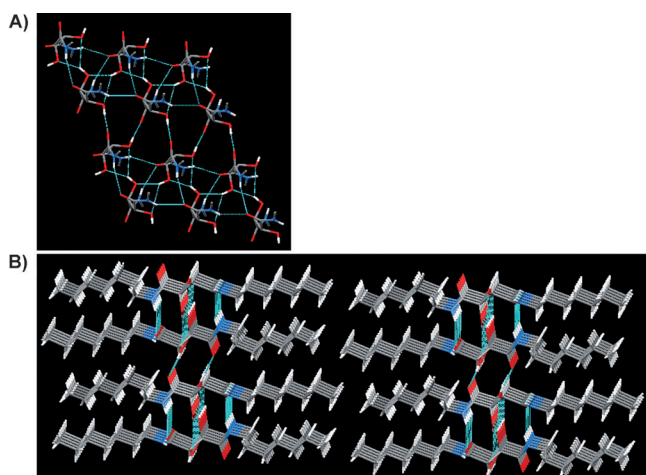


Figure 9. A) 2D hydrogen-bonding network (alkyl chains not shown for better clarity) and B) parallel packing of the 2D sheets in **DHepTA**.

in this structure, typical amide...amide-extended hydrogen bonding was not observed. Instead, one of the pyridyl N atoms participated in hydrogen bonding with the amide NH of a neighboring molecule in an extended fashion ($N\cdots N = 2.926(4) \text{ \AA}$; $\angle N-H\cdots N = 174.5^\circ$); the other pyridyl N atom did not participate in any hydrogen-bonding interactions. The hydroxyl groups in the tartaric acid backbone were involved in hydrogen bonding with the hydroxyl groups of the neighboring molecules ($O\cdots O = 3.021(4) - 2.765(4) \text{ \AA}$; $\angle O-H\cdots O = 143(4) - 147(5)^\circ$), thereby resulting in an overall 3D hydrogen-bonded network structure (Figure 10).

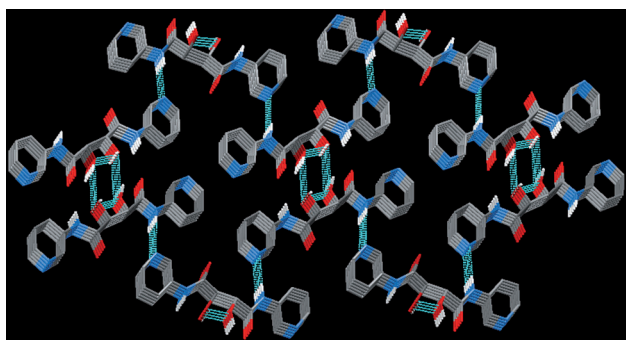


Figure 10. 3D hydrogen-bonding network illustrating N-H...N and O-H...O interactions in **D-3-PyTA**.

Single-crystal structure of DPhTA: Compound **DPhTA** was crystallized in the non-centrosymmetric orthorhombic space group $P2_12_12_1$, and its asymmetric unit contained one molecule. The chiral backbone adopted a conformation wherein the amide and the hydroxyl groups were staggered and gauche, respectively, with each other. The terminal phenyl amide moieties were nonplanar and displayed dihedral angles of 32.7 and 27.0° , and the terminal phenyl groups formed a dihedral angle of 17.3° . The amide NH moieties did not participate in any hydrogen-bonding interactions.

The hydroxyl groups were involved in extensive hydrogen bonding with the same moieties of the neighboring molecules ($O\cdots O = 2.850(3) \text{ \AA}$; $\angle O-H\cdots O = 151(3)^\circ$ and $O\cdots O = 2.9098(9) \text{ \AA}$; $\angle O-H\cdots O = 129(3)^\circ$) as well as with one of the $>C=O$ of the amide moiety ($O\cdots O = 2.650(3) \text{ \AA}$; $\angle O-H\cdots O = 162(4)^\circ$), thereby resulting in an overall 2D hydrogen-bonded network. The 2D networks were packed further in a parallel fashion (Figure 11).

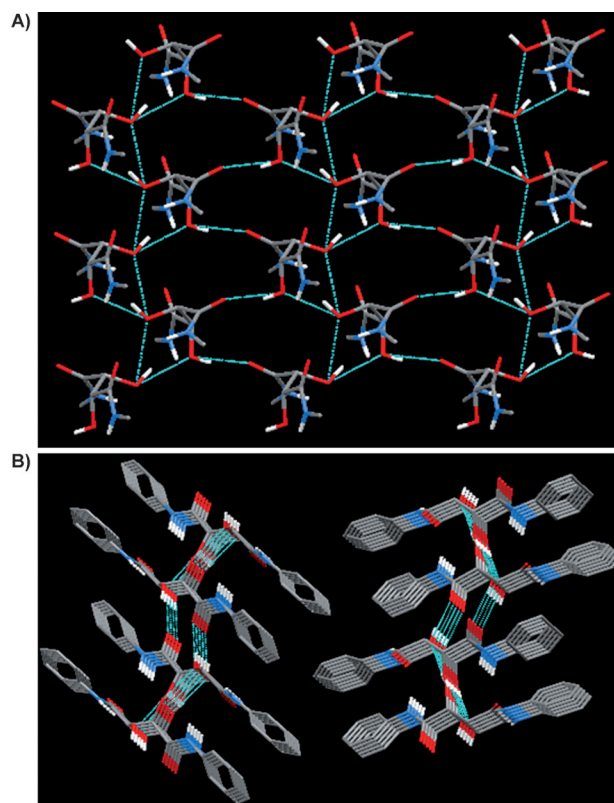


Figure 11. A) 2D hydrogen-bonding network (phenyl rings not shown for better clarity) and B) parallel packing of the 2D sheets in **DPhTA**.

Single-crystal structure of B-4-MPhTA: This compound was crystallized in the non-centrosymmetric monoclinic space group $P2_1$, and its asymmetric unit contained two molecules. The chiral backbone of both the molecules showed similar conformation wherein the amide and the hydroxyl groups were staggered and gauche, respectively, with each other. In both the molecules the terminal 4-methoxyphenyl amide moieties were nonplanar. In one molecule, the terminal 4-methoxyphenyl amide moieties displayed dihedral angles of 78.13 and 27.38° , and the terminal phenyl groups formed a dihedral angle of 2.9° . In the other molecule, the terminal 4-methoxyphenyl amide moieties showed dihedral angles of 52.11 and 17.78° , and the terminal phenyl groups displayed a dihedral angle of 51.6° . In one molecule, the amide NH moieties did not participate in any hydrogen-bonding interactions. In another molecule, only one of the amide NH moieties was involved in hydrogen-bonding interactions with one of the $>C=O$ groups of the amide moiety of the

neighboring molecule ($N\cdots O=3.056(2)$ Å; $\angle N-H\cdots O=145.5^\circ$). The hydroxyl groups were involved in extensive hydrogen bonding with the same moieties of the neighboring crystallographically equivalent molecule ($O\cdots O=2.8070(19)-2.9837(7)$ Å; $\angle O-H\cdots O=151(3)-128(2)^\circ$), the same moieties of the neighboring crystallographically nonequivalent molecule ($O\cdots O=2.6582(19)$ Å; $\angle O-H\cdots O=169(3)^\circ$), as well as with one of $>C=O$ groups of the amide moiety ($O\cdots O=2.6521(18)$ Å; $\angle O-H\cdots O=165(2)^\circ$), which resulted in an overall 2D hydrogen-bonded network. The 2D networks were packed further in parallel fashion (Figure 12).

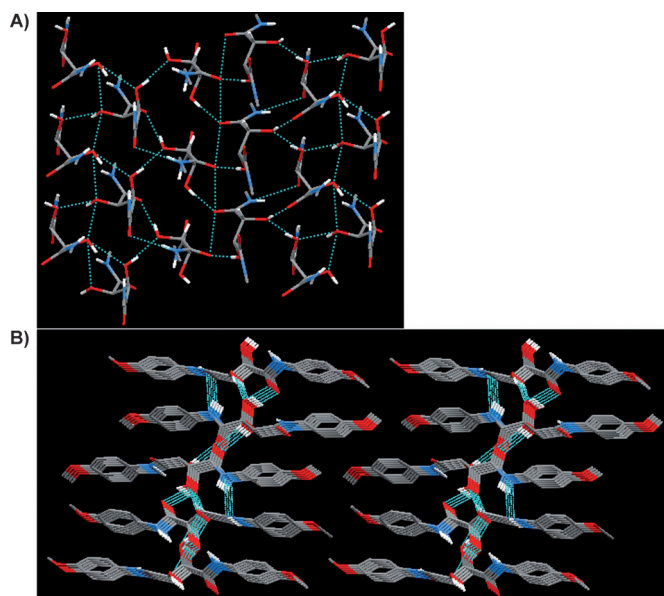


Figure 12. A) 2D hydrogen-bonding network (4-methoxyphenyl rings not shown for better clarity) and B) parallel packing of the 2D sheets in **B-4-MPhTA**.

Powder X-ray diffraction: The key to the design of any materials lies in the detailed understanding of their structures. In gel, a structural understanding of the SAFINs is key to designing gelator molecules. The detailed structural description of the SAFINs would expectedly lead to the insights into the various intermolecular interactions that involve the gelator molecules that are indispensable in the successful pursuit of designing gelators. Understandably, SXRD experiments cannot be performed with SAFINs because of their sub-X-ray size, and therefore one has to determine the structure of SAFINs by an indirect method. One such method, originally developed by Weiss et al., is employed here.^[38] In this method, the simulated, bulk, and xerogel powder X-ray diffraction (PXRD) patterns are compared; a near perfect match would indirectly determine the structural description of the SAFINs at the atomic level. It might be noted that the structure of the SAFINs present in the xerogel need not necessarily be identical with that in the gel state. During xerogel formation by evaporating a gel sample, new nucleation events might lead to the formation

of a new crystalline phase of the gelator molecule, thereby resulting in a mismatch of the corresponding PXRD patterns. However, there is no guarantee that such an event will always take place. To obtain the structure of the SAFINs in the gel state, a more powerful synchrotron beamline followed by ab initio structure determination from the PXRD data thus obtained should be employed. Since a synchrotron beamline is not so readily accessible and ab initio determination of the structure from PXRD has not yet become routine,^[39] the comparison of PXRD data of xerogel with that of bulk and simulated data is the available option. Thus, we performed PXRD experiments on selected aqueous gels of **DHepTA**, **D-3-PyTA**, and **B-4-MPhTA** as depicted in Figure 13. It was clear from the plots that in all these cases the PXRD patterns under various conditions were nearly superimposable, which meant that the single-crystal structure in respective cases actually represented the bulk as well as the SAFINs found in the xerogels.

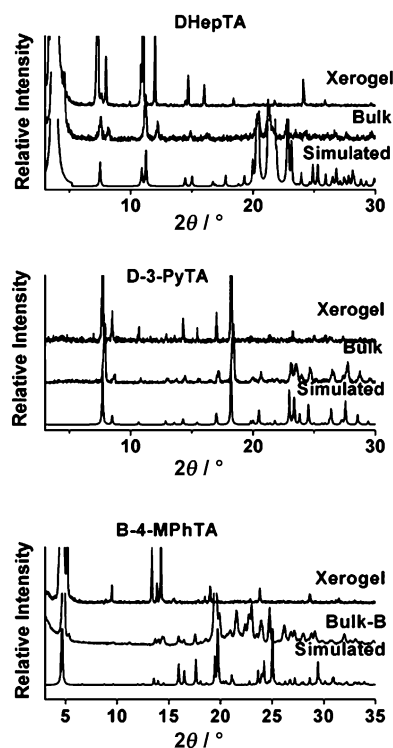
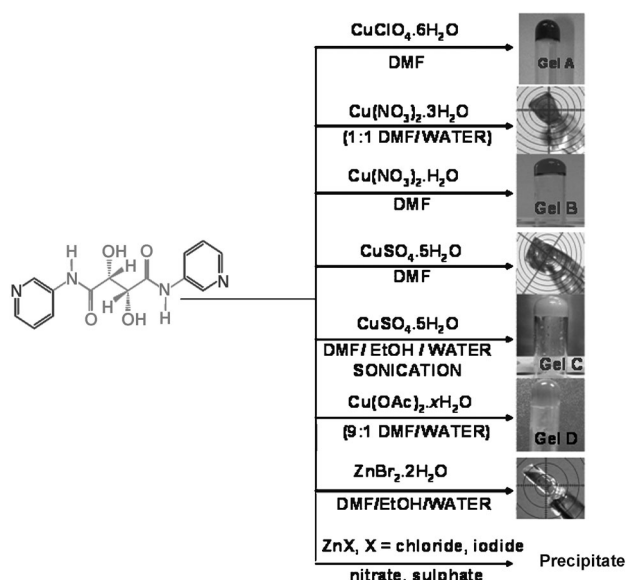


Figure 13. PXRD patterns of some of the selected gelator molecules under various conditions.

Metallogelation by D-3-PyTA: On account of its terminal 3-pyridyl rings, the gelator **D-3-PyTA** is expected to form a coordination bond with a suitable metal center and thus could be a good candidate for a metallogelling agent. When a metal takes part in the process of gelation either by coordination or being incorporated within the gel matrix as a noncoordinating metal or nanoparticle, the resulting gel is known as a metallogel.^[40] Cross-linked coordination polymers,^[41] discrete metal complexes,^[42] and well-defined coor-

dination polymers^[43] are known as metallogelators. Much effort is being directed toward metallogelation research because of the various potential applications of metallogels, such as in photophysics,^[44] catalysis,^[45] sensing,^[46] magnetic materials,^[47] and so on. Thus, we treated **D-3-PyTA** with different Cu^{II} and Zn^{II} salts under various conditions. The ligand only produced gel in DMF when treated with Cu^{II} salts in a 1:1 (metal/ligand) ratio and keeping the overall concentration within the range of 4.5–11.0 wt % (considering all the reactants) (Scheme 2). All the gels were thermorever-



Scheme 2. Metallogels and crystals obtained from **D-3-PyTA**.

sible, except gel **C** (Scheme 2) obtained from CuSO₄; in this case, the gel gradually turned into deep blue microcrystals over the period of one month. Similar reactions with Zn^{II} did not produce any gel. It may be noted that the ligand alone, being highly soluble in DMF, could not form any gel. However, it formed gel in a binary mixture of DMF/water wherein the maximum concentration of DMF was not more than 17% v/v. Dynamic rheology experiments (frequency sweep) on a selected gel (gel **B**) clearly demonstrated the typical gel-like response of gel **B**. The elastic modulus G' was frequency-invariant over a considerable frequency range and was found to be more than one order of magnitude higher than the viscous modulus G'' , thus indicating the viscoelastic behavior of gel **B** (Figure 14).

Scanning electron micrographs of these xerogels displayed highly aggregated particles instead of entangled fibers as usually observed in various xerogels (Figure 15). The solvent molecules are understandably immobilized within the gel network, thus resulting in gel formation.

As structure–property correlations on the basis of SXRD and PXRD data are often useful in understanding and designing gelators (vide supra), we attempted to crystallize some of the coordination compounds that produced gels. When a highly diluted solution of the ligand and the corre-

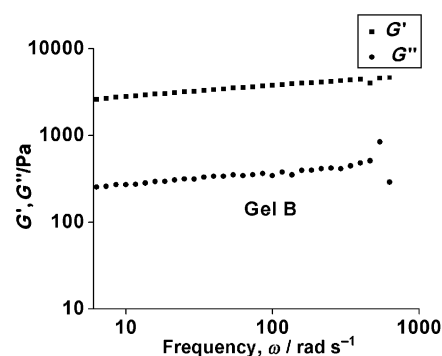


Figure 14. Dynamic rheology at 25°C of gel **B**; the elastic modulus G' and viscous modulus G'' are shown as function of the angular frequency ω . The strain used was 0.01 %.

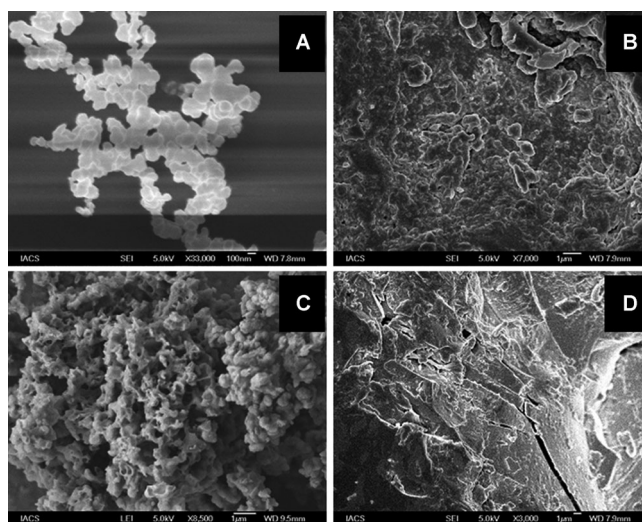


Figure 15. SEM of the DMF xerogels of A) gel **A**, B) gel **B**, C) gel **C**, and D) gel **D**.

sponding metal salts in 1:1 (metal/ligand) molar ratio in mixed solvent system was allowed to evaporate slowly, X-ray-quality single crystals were obtained (Scheme 2, Table S17 in the Supporting Information).

Crystal structure of $[(\text{H}_2\text{O})_2\text{Cu}(\mu\text{-D-3-PyTA})_2\text{Cu}(\mu\text{-D-3-PyTA})_2(\text{NO}_3)_2] \cdot (\text{NO}_3)_2 \cdot n\text{H}_2\text{O}$ (CP1): The crystals of **CP1** belong to the non-centrosymmetric tetragonal space group $P4_22_12$. In the asymmetric unit, there are two Cu atoms (both sitting at special positions with site-occupancy factors of 0.5 and 0.25), two half ligands coordinated to each Cu atom, one fully occupied nitrate coordinated to one of the Cu, and one uncoordinated disordered nitrate and one water molecule coordinated to one of the Cu atoms. Both of the Cu atoms showed slightly distorted octahedral geometry wherein the equatorial positions were coordinated by the pyridyl N atoms and the apical positions were coordinated by water in one of the Cu centers and nitrate in the other. Thus the extended coordination of the bidentate pyridyl ligand to the Cu center produced an undulating 2D grid architecture,

which were further packed in offset fashion that was sustained by hydrogen-bonding interactions that involved the amide...amide ($N\cdots O=2.935(7)$ Å; $\angle N-H\cdots N=154.4^\circ$) and hydroxyl...hydroxyl ($O\cdots O=2.795$ Å; $\angle O-H\cdots H=128.92^\circ$) interactions, which resulted in a bilayer structure. Such bilayers are further self-assembled in parallel fashion sustained by amide...amide hydrogen bonding ($N\cdots O=2.893(9)$ Å; $\angle N-H\cdots O=165.8^\circ$) (Figure 16).

Crystal structure of $[(H_2O)Cu_2(\mu-D-3-PyTA)_2(\mu-Cl)](SO_4)(Cl)_a$ (CP2): The crystals of CP2 belong to the non-centrosymmetric orthorhombic space group $F222$. The asymmetric unit contains one Cu (half-occupied), one fully occupied ligand coordinated to the metal center, one chloride (one-quarter occupied) that acts as a bridge by coordinating adjacent to the metal center, one uncoordinated sulfate (one-quarter occupied), and one uncoordinated chloride (one-quarter occupied). Although $CuSO_4$ was taken as the reacting metal salt, incorporation of chloride in the crystal structure might be due to the chloride ion present in the water used during reaction. However, we regenerated CP2 in a deliberate synthetic attempt wherein both $CuCl_2$ and $CuSO_4$ were used as metal salt as revealed in PXRD experiments (see below). A critical look into the crystal structure revealed an interesting network topology. The bipyridyl ligand coordinated to the adjacent metal center in such a way that a 1D helical coordination polymer chain was formed; such chains were further intertwined into a double helix sustained by the chloride bridge that connected the Cu centers of the adjacent helical chain. Such extended coordination ultimately led to the formation of a 2D grid wherein each side of the grid was made up of double helical chains (Figure 17). The topological analysis by TOPOS40^[48] also revealed a 5-c net; its uninodal net and topological type were found to be an sp^2 -periodic net with an extended point symbol $[4.4.4.4.4.4.4.6(3).6(3)]$ that resembled the topology of the core SnS .^[49] We could not model some electron density that arose from the solvent and it was removed by SQUEEZE,^[50] which indicated the presence of approximately twelve lattice-occluded water molecules (Figure S7 in the Supporting Information).

Crystal structure of $[(Zn_2(\mu-D-3-PyTA)_2)(Br)_2 \cdot 2DMF]_a$ (CP3): The crystals of CP3 belong to the non-centrosymmetric, orthorhombic space group $P2_12_12_1$. The asymmetric unit is comprised of two Zn atoms, two ligands, two bromide ions, and two solvate DMF molecules. The extended coordination of the ligand with the adjacent metal center produced a 1D helical chain. Such chains were further packed into 2D sheets by means of hydrogen bonding that involved hydroxyl...hydroxyl ($O\cdots O=2.855(7)$ Å; $\angle O-H\cdots H=175.3^\circ$) interactions of the ligand; the solvate DMF was found to interact with one of the amide N-H groups of the ligand backbone ($N\cdots O=2.955(8)$ Å; $\angle N-H\cdots O=155.8^\circ$) (Figure 18).

Powder X-ray diffraction: Detailed PXRD experiments were carried out on the xerogels to gain insight into the

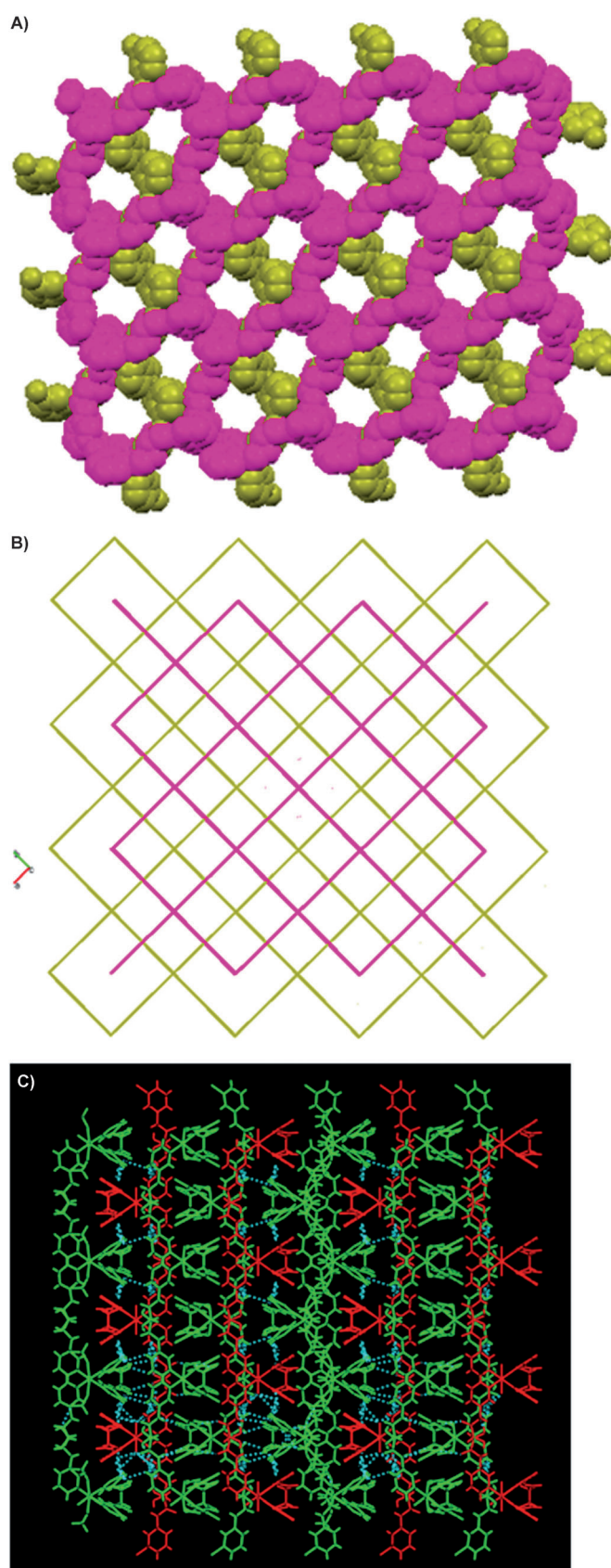


Figure 16. Single-crystal structure illustration of CP1: A) two 2D grids packed in offset fashion, B) TOPOS view of two 2D grids, and C) parallel packing of the 2D grids sustained by various hydrogen-bonding interactions marked as dotted lines.

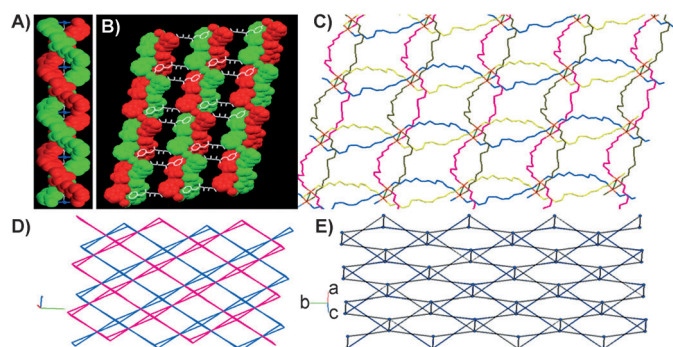


Figure 17. Single-crystal structure illustration of **CP2**: A) double-helical strand bridged by chloride, B) 2D grid composed of all double-helical sides (the horizontal sides are shown in capped stick (white)), C) another representation of a 5-c 2D network (part of the aromatic rings and hydroxyl moieties and hydrogen not shown for better clarity), D) TOPOS diagram of the 2D grid (uncoordinated chloride and sulfate not shown for better clarity), and E) TOPOS diagram of SnS.

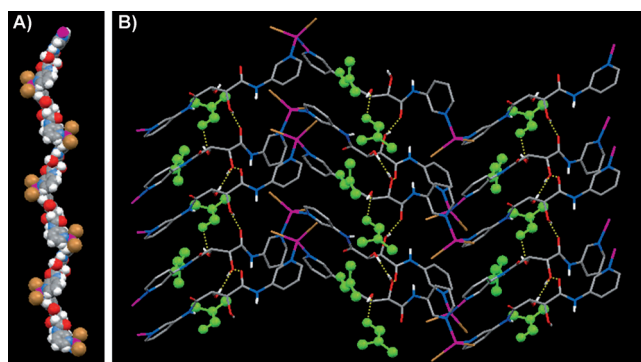


Figure 18. A) 1D helical chain and B) parallel packing of the helical chains sustained by various hydrogen-bonding interactions marked as dotted lines (solvate DMF shown in green) in **CP3**.

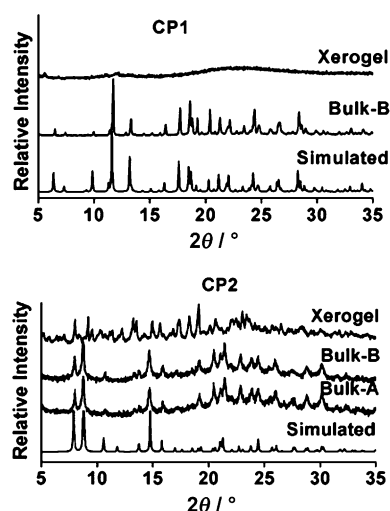


Figure 19. PXRD patterns of **CP1** and **CP2** under various conditions.

structure of the gel network in the corresponding gels for the reasons stated above (Figure 19). In **CP1**, the simulated

PXRD matched well with that of the bulk, thus indicating the high crystalline phase purity of the sample. However, the corresponding xerogel of gel **B** was found to be amorphous. In the case of **CP2**, all the PXRD patterns matched reasonably well, thereby indicating that the crystal structure of **CP2** represented the gel network in the xerogel of gel **C**. It might be mentioned here that the deliberate synthetic attempt of **CP2** by using both CuCl_2 and CuSO_4 as metal salts was successful as can be seen from the near superimposable PXRD patterns of simulated, as-synthesized bulk by using only CuSO_4 (Bulk-A), and bulk using both the Cu salts (Bulk-B) (Figure 19). The presence of chloride in **CP2** was also confirmed by energy-dispersive X-ray spectroscopy (Figure S5 in the Supporting Information). Thus, PXRD data that pertain to **CP2** clearly demonstrated that a 5-c 2D net that displayed SnS topology was responsible for the gel-forming network in gel **C**, which, to the best of our knowledge, is hitherto unknown.

Conclusion

An easy method of access to the supramolecular chirality in the form of organo-, hydro-, and metallogels has been achieved from a new series of bis-amide compounds derived from an inexpensively resourced chiral source, namely, *L*-(+)-tartaric acid. Fourteen such bis-amides have been synthesized by using various *n*-alkyl amines and a few aromatic amines, namely, 3-pyridylamine, aniline, 4-methoxyaniline, and 4-nitroaniline. Ninety-three percent of these bis-amides showed gelation with various solvents; many of them showed ambidextrous behavior. The CD spectra of some selected gels (toluene gel of **DTDTA** and DMF/water gel of **D-3-PyTA**) indicated the presence of a β -sheet-like structure in the gel state. Most of the gels displayed typical gel-like response in rheological experiments. Structure–property correlations on the basis of SXRD and PXRD data on three selected cases (DMF/water gels of **DHepTA**, **D-3-PyTA**, and **B-4-MPhTA**) established the gel-network structures in the corresponding xerogel state. One such gel (DMF/water gel of **D-3-PyTA**) displayed nanotubular morphology in the electron micrographs and has been exploited as a template to generate highly aligned silica fibers. The pyridyl-functionalized bis-amide, namely, **D-3-PyTA**, has been exploited to obtain coordination-polymer-based Cu^{II} and Zn^{II} metallogels. SXRD data of three corresponding coordination polymers (**CP1**, **CP2**, and **CP3**) have been determined and correlated with the PXRD of the corresponding xerogels. In one such case (**CP2**), the SXRD data revealed the existence of a 5-c 2D-net SnS topology in the metallogel-forming network. Interestingly, the 2D network structure was built from double helical chains sustained by a chloride bridge. To the best of our knowledge, such a 5-c 2D-net SnS topology responsible for the metallogel-forming network found in the present study is unprecedented.

Experimental Section

Materials and physical measurements: Commercially available starting materials, and reagents were used as usual without further purification. Solvents were of laboratory reagent grade and used without further distillation. Both ^1H and ^{13}C NMR spectroscopy were performed using a 300 MHz spectrometer (Bruker Avance DPX-300) and a 500 MHz spectrometer (Bruker Ultrashield Plus-500). IR spectra were obtained using an FTIR instrument (FTIR-8300, Shimadzu). The elemental compositions of the purified compounds were confirmed by elemental analysis (Perkin–Elmer Precisely, Series-II, CHNO/S Analyser-2400). SEM was recorded using a JEOL JMS-6700F field-emission scanning electron microscope. TEM was recorded using a JEOL instrument with a 300 mesh copper TEM grid. Optical microscopic pictures were taken using a Leica CLS 150X. DSC was recorded using a Perkin–Elmer Diamond DSC instrument. Rheology studies were carried out using an SDT Q series advanced rheometer AR 2000. CD were performed using a Jasco J-815 CD spectrometer. X-ray powder diffraction patterns were recorded using a Bruker AXS D8 Avance powder X-ray diffractometer ($\text{Cu}_{\text{K}\alpha 1}$ radiation, $\lambda = 1.5406 \text{ \AA}$).

Caution! All the aliphatic amines used for the corresponding amide synthesis are highly volatile, and inhalation of this compound might cause severe burns to the mucous membrane tissue. Therefore it should be handled with care.

Gel–sol dissociation temperature (T_{gel}) measurement: We used a dropping-ball method to determine T_{gel} . A locally made glass ball that weighed 306.0 mg was kept on the gel (0.5 mL) placed in a test tube (10 × 100 mm). The tube was immersed in an oil bath placed on a magnetic stirrer to ensure uniform heating. The temperature at which the ball reached the bottom of the tube was considered to be T_{gel} .

SEM and TEM: Dilute (0.5 wt %) solution of the corresponding gelators were drop cast on the glass plate fixed with the standard metallic SEM stub and dried under ambient conditions. The samples were coated with platinum, and the SEM images were recorded. The sample for TEM was prepared by depositing a drop of a dilute solution (on the order of 10^{-2}M) on a carbon-coated Cu (300 mesh) TEM grid. The grid was dried under vacuum at room temperature for one day and used for recording TEM images using an accelerating voltage of 80 kV.

Single-crystal X-ray diffraction: X-ray-quality single crystals were obtained by a slow evaporation method at room temperature. Whereas **D-3-PyTA** was crystallized from a DMF/MeOH solution, crystals of **DHepTA** were obtained from an MeOH solution. Crystals of **DPhTA** were obtained from a DMSO/acetonitrile mixture, whereas **B-4-MPhTA** was crystallized from *p*-xylene. A single crystal of **CPI** was obtained when a DMF/water solution of **D-3-PyTA** and $\text{Cu}(\text{NO}_3)_2$ were allowed to evaporate. Both **CP2** and **CP3** were obtained when a solution of **D-3-PyTA** in DMF/ethanol was layered atop the aqueous solution of CuSO_4 and ZnBr_2 , respectively, and allowed to evaporate slowly.

Single-crystal X-ray data were collected with $\text{Mo}_{\text{K}\alpha}$ radiation ($\lambda = 0.7107 \text{ \AA}$) using a SMART APEX-II diffractometer equipped with a CCD area detector. Data collection, data reduction, and structure solution and refinement were carried out using the SMART APEX-II software package. All the structures were solved by direct methods and refined in a routine manner. In all cases, non-hydrogen atoms were treated anisotropically. Whenever possible, the hydrogen atoms were located on a difference Fourier map and refined. In other cases, the hydrogen atoms were geometrically fixed at their idealized positions.

CCDC-812385, -812385, -812385 and -812385 contain the supplementary crystallographic data for this paper. These data can be obtained free of charge from The Cambridge Crystallographic Data Centre via www.ccdc.cam.ac.uk/data_request/cif.

Acknowledgements

U.K.D. and P.D. thank CSIR, New Delhi for a Senior Research Fellowship (SRF) and financial support, respectively. All the single-crystal X-ray diffraction data were collected at the DST-funded National Single Crystal Diffractometer facility at the Department of Inorganic Chemistry, IACS, Kolkata.

- [1] a) P. Terech, R. G. Weiss, *Chem. Rev.* **1997**, *97*, 3133–3160; b) *Molecular Gels: Materials with Self-Assembled Fibrillar Networks* (Eds.: R. G. Weiss, P. Terech), Springer, Dordrecht, **2005**.
- [2] E. Carretti, M. Bonini, L. Dei, B. H. Berrie, L. V. Angelova, P. Baglioni, R. G. Weiss, *Acc. Chem. Res.* **2010**, *43*, 751–760.
- [3] E. Carretti, L. Dei in *Molecular Gels: Materials with Self-Assembled Fibrillar Networks* (Eds.: G. Weiss, P. Terech), Springer, Dordrecht, **2005**, Chapter 27, pp. 929–938.
- [4] a) T. Kato, *Science* **2002**, *295*, 2414–2418; b) A. Ajayaghosh, V. K. Praveen, C. Vijayakumar, S. George, *Angew. Chem.* **2007**, *119*, 6376–6381; *Angew. Chem. Int. Ed.* **2007**, *46*, 6260–6265; c) A. Ajayaghosh, C. Vijayakumar, V. K. Praveen, S. Santhosh Babu, R. Varghese, *J. Am. Chem. Soc.* **2006**, *128*, 7174–7175.
- [5] a) K. J. C. van Bommel, A. Friggeri, S. Shinkai, *Angew. Chem.* **2003**, *115*, 1010–1030; *Angew. Chem. Int. Ed.* **2003**, *42*, 980–999; b) H. Basit, A. Pal, S. Sen, S. Bhattacharya, *Chem. Eur. J.* **2008**, *14*, 6534–6545; c) S. Ray, A. K. Das, A. Banerjee, *Chem. Commun.* **2006**, 2816–2818; d) G. Gundiah, S. Mukhopadhyay, U. G. Tumkurkar, A. Govindaraj, U. Maitra, C. N. R. Rao, *J. Mater. Chem.* **2003**, *13*, 2118–2122.
- [6] a) A. Wynne, M. Whitefield, A. J. Dixon, S. Anderson, *J. Dermatol. Treat.* **2002**, *13*, 61–66; b) V. Jennings, A. Gysler, M. Schafer-Korting, S. H. Gohla, *Eur. J. Pharm. Biopharm.* **2000**, *49*, 211–218.
- [7] Z. Yan, G. Liang, L. Wang, B. Xu, *J. Am. Chem. Soc.* **2006**, *128*, 3038–3043.
- [8] K. Y. Lee, D. J. Mooney, *Chem. Rev.* **2001**, *101*, 1869–1880.
- [9] a) K. Murata, M. Aoki, T. Nishi, A. Ikeda, S. Shinkai, *J. Chem. Soc. Chem. Commun.* **1991**, 1715–1718; b) J. J. D. de Jong, L. N. Lucas, R. M. Kellogg, J. H. van Esch, B. L. Feringa, *Science* **2004**, *304*, 278–281.
- [10] a) A. Ballabh, D. R. Trivedi, P. Dastidar, *Chem. Mater.* **2006**, *18*, 3795–3800; b) S. Bhattacharya, Y. K. Ghosh, *Chem. Commun.* **2001**, 185–186; c) S. R. Jadhav, P. K. Vemula, R. Kumar, S. R. Raghavan, G. John, *Angew. Chem.* **2010**, *122*, 7861–7864; *Angew. Chem. Int. Ed.* **2010**, *49*, 7695–7698.
- [11] B. Escuder, F. R. Llansola, J. F. Miravet, *New J. Chem.* **2010**, *34*, 1044–1054.
- [12] a) Y.-C. Lin, R. G. Weiss, *Macromolecules* **1987**, *20*, 414–417; b) ref. [9a]; c) R. Mukkamala, R. Weiss, *Langmuir* **1996**, *12*, 1474–1482; d) C. Geiger, M. Stabescu, L. Chen, D. G. Whitten, *Langmuir* **1999**, *15*, 2241–2245.
- [13] a) W. Gu, L. Lu, G. B. Chapman, R. G. Weiss, *Chem. Commun.* **1997**, 543–544; b) ref. [27].
- [14] a) P. Terech, P. Gebel, R. Ramasseul, *Langmuir* **1996**, *12*, 4321–4323; b) H. Engelkamp, S. Middelbeek, R. J. M. Nolte, *Science* **1999**, *284*, 785–788.
- [15] a) S. Yamamoto, *J. Soc. Chem. Ind. Jpn.* **1943**, *46*, 279–281 (CA46: 7047h); b) F. R. Taravel, B. PfannemueLLer, *Makromol. Chem.* **1990**, *191*, 3097–3106; c) S. Yamasaki, H. Tsutsumi, *Bull. Chem. Soc. Jpn.* **1994**, *67*, 2053–2056; d) R. J. H. Hafkamp, M. C. Feiters, R. J. M. Nolte, *J. Org. Chem.* **1999**, *64*, 412–426; e) U. Beginn, S. Keinath, M. Möller, *Macromol. Chem. Phys.* **1998**, *199*, 2379–2384; f) K. Yoza, N. Amanokura, Y. Ono, T. Akao, H. Shinmori, S. Shinkai, D. N. Reinhoudt, *Chem. Eur. J.* **1999**, *5*, 2722–2729.
- [16] a) E. J. de Vries, R. M. Kellogg, *J. Chem. Soc. Chem. Commun.* **1993**, 238–240; b) K. Hanabusa, J. Tange, Y. Taguchi, T. Koyama, H. Shirai, *J. Chem. Soc. Chem. Commun.* **1993**, 390–392; c) A. Aggeli, M. Bell, N. Boden, J. N. Keen, P. F. Knowles, T. C. B. McLeish, M. Pitkeathly, S. E. Radford, *Nature* **1997**, *386*, 259–262.

- [17] a) K. Hanabusa, K. Shimura, K. Hirose, M. Yamada, H. Shirai, *Chem. Lett.* **1996**, 885–886; b) H. Shi, Z. Huang, S. Kilic, J. Xu, R. M. Enick, E. J. Beckman, A. J. Carr, R. E. Melendez, A. D. Hamilton, *Science* **1999**, 286, 1540–1543; c) J. H. van Esch, S. De Feyter, R. M. Kellogg, F. De Schryver, B. L. Feringa, *Chem. Eur. J.* **1997**, 3, 1238–1243; d) M. de Loos, J. H. van Esch, I. Stokroos, R. M. Kellogg, B. L. Feringa, *J. Am. Chem. Soc.* **1997**, 119, 12675–12676; e) J. H. van Esch, F. Schoonbeek, M. de Loos, H. Kooijman, A. L. Spek, R. M. Kellogg, B. L. Feringa, *Chem. Eur. J.* **1999**, 5, 937–950.
- [18] K. J. C. van Bommel, C. van der Pol, I. Muizebelt, A. Friggeri, A. Heeres, A. Meetsma, B. L. Feringa, J. van Esch, *Angew. Chem.* **2004**, 116, 1695–1699; *Angew. Chem. Int. Ed.* **2004**, 43, 1663–1667.
- [19] P. Dastidar, *Chem. Soc. Rev.* **2008**, 37, 2699–2715.
- [20] a) P. Guo, L. Zhang, M. Liu, *Adv. Mater.* **2006**, 18, 177–180; b) H. Goto, E. Yashima, *J. Am. Chem. Soc.* **2002**, 124, 7943–7949; c) Y. Li, T. Wang, M. Liu, *Soft Matter* **2007**, 3, 1312–1317.
- [21] F. Rodríguez-Llansola, J. F. Miravet, B. Escuder, *Chem. Commun.* **2009**, 7303–7305.
- [22] a) H. Ihara, M. Takafuji, T. Sakurai in *Encyclopedia of Nanoscience and Nanotechnology*, Vol. 9 (Ed.: H. S. Nalwa), American Scientific Publishers, Stevenson Ranch, **2004**, p.473; b) A. Brizard, R. Oda, I. Huc, *Top. Curr. Chem.* **2005**, 256, 167–218; c) J. M. Schnur, *Science* **1993**, 262, 1669–1676.
- [23] J. Bunzen, U. Kiehne, C. Benkhäuser-Schunk, A. Lützen, *Org. Lett.* **2009**, 11, 4786–4789.
- [24] P. Sahoo, D. K. Kumar, S. R. Raghavan, P. Dastidar, *Chem. Asian J.* **2011**, 6, 1038–1047.
- [25] a) J. D. Hartgerink, E. Beniash, S. I. Stupp, *Proc. Natl. Acad. Sci. USA* **2002**, 99, 5133–5138; b) T. Aida, E. W. Meijer, S. I. Stupp, *Science* **2012**, 335, 813–817.
- [26] J. C. MacDonald, G. M. Whitesides, *Chem. Rev.* **1994**, 94, 2383–2420.
- [27] R. Oda, I. Huc, S. Candau, *Angew. Chem.* **1998**, 110, 2835–2838; *Angew. Chem. Int. Ed.* **1998**, 37, 2689–2691.
- [28] W. Chen, Y. Liu, Z. Chen, *Eur. J. Org. Chem.* **2005**, 1665–1668.
- [29] A material is considered a gel if no deformity of the material is observed after inverting the tube that contains the material.
- [30] a) Y. Ji, Y. F. Luo, X. R. Jia, E. Q. Chen, Y. Huang, C. Ye, B. B. Wang, Q. F. Zhou, Y. Wei, *Angew. Chem.* **2005**, 117, 6179–6183; *Angew. Chem. Int. Ed.* **2005**, 44, 6025–6029; b) G. C. Kuang, Y. Ji, X. R. Jia, Y. Li, E. Q. Chen, Y. Wei, *Chem. Mater.* **2008**, 20, 4173–4175.
- [31] S. R. Raghavan, B. H. Cipriano in *Molecular Gels: Materials with Self-Assembled Fibrillar Networks* (Eds.: G. Weiss, P. Terech), Springer, Dordrecht, **2005**, Chapter 8, pp. 241–252.
- [32] B. G. Bag, S. K. Dinda, P. P. Dey, V. A. Mallia, R. G. Weiss, *Langmuir* **2009**, 25, 8663–8671.
- [33] S. A. Khan, J. R. Royer, S. R. Raghavan, *Aviation Fuels with Improved Fire Safety: A Proceedings* **1997**, 6, 31–46.
- [34] N. Sreerama, R. W. Woody in *Circular Dichroism: Principles and Applications* (Eds.: N. Beroba, K. Nakanishi, R. W. Woody), Wiley, New York, **2000**, pp. 601–620.
- [35] a) D. K. Kumar, D. A. Jose, A. Das, P. Dastidar, *Chem. Commun.* **2005**, 4059–4061; b) S. Kiyonaka, K. Sada, I. Yoshimura, S. Shinkai, N. Kato, I. Hamachi, *Nat. Mater.* **2004**, 3, 58–64.
- [36] R. Luboradzki, O. Gronwald, M. Ikeda, S. Shinkai, D. N. Reinhoudt, *Tetrahedron* **2000**, 56, 9595–9599.
- [37] a) D. R. Trivedi, A. Ballabh, P. Dastidar, B. Ganguly, *Chem. Eur. J.* **2004**, 10, 5311–5322; b) U. K. Das, D. R. Trivedi, N. N. Adarsh, P. Dastidar, *J. Org. Chem.* **2009**, 74, 7111–7121.
- [38] E. Ostuni, P. Kamaras, R. G. Weiss, *Angew. Chem.* **1996**, 108, 1423–1425; *Angew. Chem. Int. Ed. Engl.* **1996**, 35, 1324–1326.
- [39] P. Martinetto, P. Terech, A. Grand, R. Ramassoul, E. Dooryhée, M. Anne, *J. Phys. Chem. A J. Phys. Chem. B.* **2006**, 110, 15127–15133.
- [40] a) B. Xing, M.-F. Choi, B. Xu, *Chem. Commun.* **2002**, 362–363; b) M. O. M. Piepenbrock, G. O. Lloyd, N. Clarke, J. W. Steed, *Chem. Rev.* **2010**, 110, 1960–2004.
- [41] K. Hanabusa, Y. Maesaka, M. Suzuki, M. Kimura, H. Shirai, *Chem. Lett.* **2000**, 1168–1169.
- [42] a) Ref. [14a]; b) M. Kimura, T. Muto, H. Takimoto, K. Wada, K. Ohta, K. Hanabusa, H. Shirai, N. Kobayashi, *Langmuir* **2000**, 16, 2078–2082; c) T. Ishi-I, R. Iguchi, E. Snip, M. Ikeda, S. Shinkai, *Langmuir* **2001**, 17, 5825–5833; d) D. López, J.-M. Guenet, *Macromolecules* **2001**, 34, 1076–1081.
- [43] P. Terech, V. Schaffhauser, P. Maldivi, J. M. Guenet, *Langmuir* **1992**, 8, 2104–2106.
- [44] a) A. Kishimura, T. Yamashita, K. Yamaguchi, T. Aida, *Nat. Mater.* **2005**, 4, 546–549; b) M. Shirakawa, N. Fujita, T. Tani, K. Kaneko, S. Shinkai, *Chem. Commun.* **2005**, 4149–4151; c) S. Kume, K. Kuroiwa, N. Kimizuka, *Chem. Commun.* **2006**, 2442–2444; d) A. Y.-Y. Tam, K. M.-C. Wong, G. Wang, V. W.-W. Yam, *Chem. Commun.* **2007**, 2028–2030.
- [45] B. Escuder, J. F. Miravet, *Chem. Commun.* **2005**, 5796–5798.
- [46] S. R. Bull, M. O. Guler, R. E. Bras, T. J. Meade, S. I. Stupp, *Nano Lett.* **2005**, 5, 1–4.
- [47] O. Roubeau, A. Colin, V. Schmitt, R. Clerac, *Angew. Chem.* **2004**, 116, 3345–3348; *Angew. Chem. Int. Ed.* **2004**, 43, 3283–3286.
- [48] V. A. Blatov, D. M. Proserpio, TOPOS 4.0, A program package for multipurpose crystallochemical analysis.
- [49] a) ICSD Code 15737; b) K. M. Blake, A. Banisafar, R. L. LaDuca, *Inorg. Chim. Acta* **2011**, 373, 201–210.
- [50] P. Van der Sluis, A. L. Spek, *Acta Crystallogr. Sect. A* **1990**, 46, 194–201.

Received: March 15, 2012

Revised: June 25, 2012

Published online: September 7, 2012

Please note: Minor changes have been made to this manuscript since its publication in *Chemistry—A European Journal* Early View. The Editor.